Available online at www.sciencedirect.com
ScienceDirect
Polymer 48 (2007) 598–615
polymer
www.elsevier.com/locate/polymer

The mechanical properties of poly(ether-ether-ketone) (PEEK) with emphasis on the large compressive strain response

P.J. Rae [a,*], E.N. Brown [a], E.B. Orler [b]

[a] Los Alamos National Laboratory (LANL), Structure Property Relations, MST-8, MS-G755, P.O. Box 1663, Los Alamos, NM 85745, United States
[b] Los Alamos National Laboratory, Polymers and Coatings Group, MST-7, MS-E549, P.O. Box 1663, Los Alamos, NM 85745, United States

Received 21 September 2006; received in revised form 13 November 2006; accepted 15 November 2006
Available online 15 December 2006

Abstract

The mechanical properties of PEEK 450G have been extensively investigated. The compressive properties were measured at strain rates between 1×10^{-4} and 3000 s^{-1} and temperatures between −85 and 200 °C. The tensile properties were measured between the strain rates of 2.7×10^{-5} and 1.9×10^{-2} s^{-1} and at temperatures between −50 and 150 °C. The Taylor impact properties were investigated as a function of velocity and various large-strain compression tests were undertaken to explain the results. The fracture toughness was investigated as a function of temperature and compared with previous literature. Additionally, the fracture surfaces were studied by microscopy. As with all semi-crystalline polymers the mechanical response is a strong function of the strain rate and testing temperature. A previously reported phenomenon of darkening observed in Taylor impacted samples is shown to be due to reduced crystallinity brought about by large compressive strain. For samples deformed to large compressive strains using a variety of techniques and strain-rates the measured Vickers hardness was found to decrease in accordance with reduced crystallinity measured by other techniques.

Keywords: Poly(ether-ether-ketone) (PEEK); Tension and compression; Large-strain discolouration

1. Introduction

Poly(ether-ether-ketone) (PEEK) is a relatively new semi-crystalline polymer first appearing in the literature in the early 1980s [1]. It also appears in the literature as poly(aryl-ether-ether-ketone) although its true scientific name is poly(oxy-1,4-phenylene-oxy-1,4-phenylenecarbonyl-1,4-phenylene). It has a high melt and glass transition temperatures (T_m = 340 °C, T_g = 143 °C), high chemical resistance and is melt processable. Thus it has been used in a variety of structural and insulation applications. A considerable body of literature exists on a number of topics related to PEEK mechanical properties. PEEK crystallizes rapidly at temperatures above T_g. This results in difficulty in performing absolute differential scanning calorimetry (DSC) to establish crystallinity and melt temperatures because the samples crystallinity increases during the scan. A number of investigators have looked at this problem. Jonas et al. [2] correlated DSC scans to density and infrared measurements of crystallinity. Sauer et al. [3] investigated a number of polymers exhibiting double melt endotherms to understand the equilibrium melt temperature, while Wei et al. undertook a careful analysis of the causes of the double melt endotherm [4]. The whole topic of measuring crystallinity of polymers by DSC is discussed by Kong and Hay [5]. The crystal structure has been studied by various researchers [6–9], while Bas et al. [10] have studied the crystallization kinetics.

The tensile properties have been examined by a number of authors [11–15] while the compressive properties over a wide range of strain rates have been studied by Cady et al. [16], Hamdan and Swallowe [17–19] and Walley et al. [20]. Bas and Alberola [21] used DMA to investigate the dynamic mechanical properties of PEEK in various solvents while Ivanov and Jonas used the DMA technique to examine the glass transition [62].

* Corresponding author. Tel.: +1 5056674436.
E-mail address: prae@lanl.gov (P.J. Rae).

0032-3861/$ - see front matter © 2006 Elsevier Ltd. All rights reserved.
doi:10.1016/j.polymer.2006.11.032

The shock properties appear not to have been studied, except for two recent papers by Millett et al. [22,23].

The most complete study of the compressive properties of PEEK is described in a series of papers by Hamdan and Swallowe [17–19]. They studied PEEK 150G by varying the starting crystallinity, temperature and altering the testing strain-rate. It was found that at lower strain rates ($<10^3\ s^{-1}$) the crystallinity of samples decreased when deformed to peak true strains of approximately 60%, but at strain rates above this value the crystallinity increased, particularly when the specimen starting temperature was greater than 80 °C. The yield stress associated with tests at rates above $10^3\ s^{-1}$ also rapidly increased deviating from the linearly increasing trend at lower rates. The perfection of crystallites was found to be greater in samples tested at high rates and high temperatures ($>T_g$). Hamdan and Swallowe postulated that this occurs because of the adiabatic nature of the high strain-rate tests leading to sample heating and associated annealing.

Despite the relatively high fracture toughness of PEEK, the majority of investigations on fracture behavior has focused on carbon fiber reinforced PEEK composites [24–28]. However, a number of studies have been published using linear-elastic fracture mechanics (LEFM) with a compact tension geometry [29–34], a three-point bend technique [35,36,33], or a single edge notched tensile (SENT) specimen [11]. These studies are primarily focused on moderate loading rates and at room temperature, agreeing on a G_{IC}[1] fracture toughness of 8–12 kJ m^{-2} under these conditions. Fatigue failure [37,31,38] and high rate fracture by Charpy impact [39] have also been investigated. Beguelin and Kausch [32] and Gensler et al. [33] both reported a strong logarithmic decrease in critical stress intensity with loading rate. Hashemi [40] and Arkhireyeva and Hashemi [41] have recently employed the essential work of fracture (EWF) analysis to PEEK over a range of temperatures. However, this method homogenizes the energy involved in numerous mechanical events including elastic and plastic deformations, localized necking, crack initiation, crack growth and finally failure. As such, determining a fracture criterion or comparing the data to rigorously obtained fracture data is nearly impossible. In fact these studies report critical energy values that are 150–300% above that of all other work in the literature. At least, in part, the inconsistency in their data may result from the fact that, as pointed out by Karger-Kocsis [42], the EWF method has several limitations for polymers. Not least of these is that complete yielding of the ligament must occur prior to any crack initiation, which can only rigorously be achieved in amorphous polymers. To the best of the authors' knowledge, the only other investigation on the fracture behavior of PEEK over a wide range of temperatures was performed by Karger-Kocsis and Friedrich [29]. However, they restricted their measurement technique to LEFM, which they acknowledged did not accurately capture the material behavior at elevated temperatures or rates. To overcome these issues, in the current work the authors' employ the single-specimen, *J*-integral normalization technique to capture the full elastic–plastic response of PEEK during fracture from −50 to 150 °C.

The Taylor test [43] involves firing a right cylinder of test material against a semi-infinite rigid anvil. The test was originally posed as a method for measuring the dynamic yield strength of metals, however, more recently it has been used as a dynamic validation tool for computer based models. When coupled with high-speed photography the response of visco-elastic materials such as polymers can be measured [44–47]. Recently Millett et al. published an investigation on the Taylor response of an unspecified grade of commercially supplied PEEK [47]. A number of interesting findings were noted relating to the ductile nature of the material in this test and material discolouration in the vicinity of the most deformed areas. Millett et al. report that at velocities between 152 and 349 m s^{-1} PEEK failed in a ductile manner with increasing mushrooming of the impact zone and tearing. At a velocity of 408 m s^{-1} a sufficient tensile stress was developed behind the impact zone to cause a ductile failure of the rod. Concave rod ends revealed significant post impact relaxation. Discolouration was noted in the rod end regions exhibiting the greatest residual deformation, which Millett et al. attributed to either shock- and strain-heating or an oxidation process from the air present during the impact.

2. Materials

A commercial plate of extruded PEEK 450G was purchased measuring $475 \times 475 \times 19\ mm^3$. The material has been characterized in tension and compression at various temperatures and strain rates. Using helium pycnometry a density of $\rho = 1311 \pm 1\ kg\ m^3$ was measured. The crystallinity calculated from density is $39 \pm 2\%$ [10]. From differential scanning calorimetry (DSC) a material crystallinity of $41 \pm 2\%$ was calculated by integrating the melt endotherm and relating it to the literature value for 100% crystalline PEEK 450G [2].

Estimates of the molecular weight of the PEEK samples were undertaken by Polymer Solutions Inc., Virginia, USA using the dissolved viscosity method from Devaux et al. [48]. Samples were dissolved in concentrated sulphuric acid and allowed to stand for equal lengths of time to normalize the sulphonation of the polymer chains. Viscosity measurements were calculated according to ASTM D2857-95(2001) at 30 °C. Devaux et al. provide a plot of weight averaged molecular weights versus intrinsic viscosity and this was used to estimate the molecular weight of our as received PEEK. It indicates a weight averaged molecular weight of ≈28 000.

3. Experimental

3.1. Differential scanning calorimetry (DSC)

Thermal properties were measured using a TA Instruments Q1000 DSC. Samples (ca. 10 mg) were loaded and sealed in

[1] In all cases the reported studies assumed linear elasticity and thus reported fracture toughness as K_{IC} with values from 5.4 to 7.5 MPa m$^{1/2}$. Where possible, values of E reported to correspond to the material investigated were used for $G_{IC} = K_{IC}^2/E$, when not reported $E = 4.10$ GPa was used.

standard DSC pans and cooled to −145 °C. They were scanned at a rate of 10 °C min^{-1} under a nitrogen purge. As explained in Section 1, measuring the absolute crystallinity in PEEK via DSC is difficult owing to the rapid crystallization kinetics. For the purposes of this study, relative crystallinities of the tested samples were felt to be more important than absolute values. Therefore, the percentage of crystallinity was estimated by the most simple means of integrating the melt endotherm or endotherms (measured heat of fusion, H_f) and calculating the ratio with a theoretical 100% crystalline sample (ΔH_f^0). Jonas et al. [2] estimated ΔH_f^0 to be 130 J g^{-1} and this value is used throughout this paper.

3.2. Dynamic mechanical analysis (DMA)

The loss factor, tan δ was measured as a function of temperature by DMA and the in-phase elastic (storage) shear modulus (G') and loss modulus (G'') were calculated. Samples were analyzed in the shear mode using a TA Instruments ARES. Sample bars were machined to 1.5 mm thick by 10 mm wide and 15 mm long. Frequency/temperature sweeps were obtained from 0.1 to 100 rad s^{-1} at 0.1% strain under a nitrogen purge from 50 to 200 °C. The G' and tan δ results are shown in Fig. 1.

3.3. Tension and compression testings

Given the ductile nature of PEEK in compression, samples were deformed to large strains in many cases. For this reason, all strains referenced in this paper, unless otherwise noted, are true strains (logarithmic strains). A constant loading strain-rate was maintained for all large-strain compression experiments. The feedback loop from the testing machines was closed to correctly slow the crosshead as the samples thinned. True-stress was calculated assuming a constant sample volume.

The compression sample geometry chosen was 6.375 mm in diameter by 6.375 mm long right-regular cylinders. The aspect ratio of 1:1 is smaller than the 1:1.5−1:2 values often employed in compression tests on metals but the sample size and ratio were therefore chosen to conserve material for the large number of tests required.

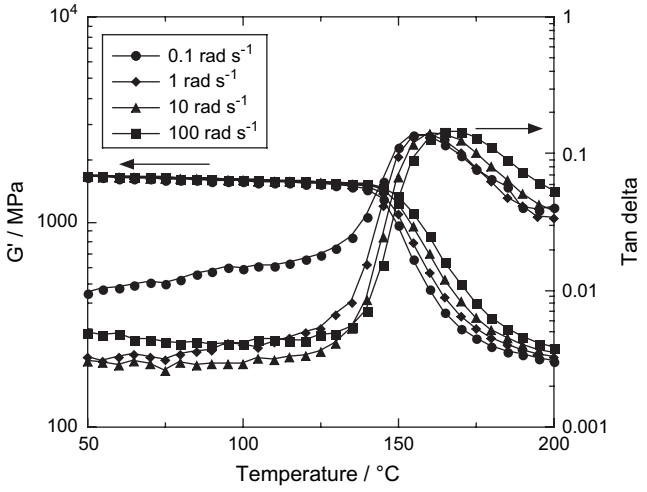

Fig. 1. PEEK 450G shear DMA results at four rates from 50 to 200 °C.

For lower strain-rate compression tests a MTS 880 servo-hydraulic machine was utilized. A MTS 810 machine with a 180 gal per minute servo valve was used for strain rates of 10 and 100 s^{-1}. These machines ran MTS TestStar software also allowing for full control over the test profile. In all samples tested at −20 °C, or higher, paraffin wax was used to lubricate the specimen ends [49,20]. The specimens were compressed between highly polished tungsten carbide platens to further lower the friction. Temperature control was carried out using either electrically heated or liquid nitrogen cooled platens and surrounding insulation was used to create a small environmental chamber. The samples were allowed to equilibrate at temperature between 30 and 45 min prior to testing.

For the tensile experiments, a screw driven Instron 4482 frame was used. This machine has been fitted with a modern PC control system (MTS Testworks 4[2]) allowing a wide range of control modes and input channels. Samples were machined to form ASTM D-638 Type V specimens. All specimens were allowed to equilibrate at the testing temperature between 45 and 100 min prior to tensile testing. It was discovered that at all temperatures and strain rates tested here the true strain to failure was limited to less than 0.6. More importantly after a linear-elastic type loading, a load drop occurs as a neck forms. Upon necking the sample is no longer in a uniaxial stress state and the data generated are essentially invalid except to verify predictions from a full three-dimensional computer model. To obtain accurate data on the uniaxial part of the curve, an Instron 2620 extensometer was utilized. This had a gauge length of 9.2 mm and a maximum displacement of 5.08 mm, leading to a maximum sample true strain of 0.44. Since, in tension, valid data are only obtained for strains less than 6%, plots are made in engineering stress and strain to indicate the loss of uniaxial loading. At low strains before the necking point, true and engineering values are essentially identical.

For high strain-rate compression testing (3000 ± 200 s^{-1}), a LANL-built split-Hopkinson pressure bar was used [50]. This Hopkinson bar is fitted with a small environmental chamber surrounding the test sample. In the chamber, either heated or cooled gas can be introduced to vary the sample temperature between −100 and +150 °C. The change in impedance at the ends of the Ti−6Al−4V bars used for testing in this temperature range is negligible. As before, paraffin wax was used to lubricate the specimen ends for all samples tested at −20 °C or higher. No lubricant was used at lower temperatures, but owing to the relatively small strains imposed on the sample and the low coefficient of friction between PEEK and the finely finished pressure bars, no sample barreling was found.

A custom built 6 m drop tower was used for the intermediate strain-rate tests to large strains and the residual true strain was measured from the starting and relaxed dimensions of the

[2] <http://www.mts.com/>.

sample while the quoted strain-rate is an average of the measurement throughout the test.

3.4. Hardness testing

Micro-hardness measurements were made on a Buehler Micromet hardness tester using the Vickers geometry with a 25 g load and 20 s dwell time. The samples to be tested were mounted in epoxy and polished using successively finer grits finishing with 0.3 μm alumina. In this way a flat and smooth surface was created that allowed reproducible data to be obtained. Depending on the size of the region of interest, readings between 3 and 9 sites were averaged to obtain the quoted values.

3.5. Ultrasonic sound speed measurements

The speed of sound in PEEK was measured using a time of flight method [51]. Room temperature samples of 19 mm thick were tested using longitudinal and shear wave inducing heads.[3] Correcting for the triggering, cable and transducer and coupling medium delays (220 ns for the shear transducer and 260 ns for the longitudinal one), the results are shown in Table 1. Values for Young's modulus (E), Poisson's ratio (ν), shear modulus (G' or G) and bulk modulus (K) are obtained using the material density quoted above and the following expressions:

$$E = 2\rho C_s^2(1+\nu) \tag{1}$$

$$\nu = \frac{C_l^2 - 2C_s^2}{2\left(C_l^2 - C_s^2\right)} \tag{2}$$

$$G = \frac{E}{2(1+\nu)} \tag{3}$$

$$K = \frac{E}{3(1-2\nu)} \tag{4}$$

where C_l and C_s are the longitudinal and shear wave-speeds, respectively, and ρ is the density. These expressions are only valid for isotropic solids within the elastic region, but given the minute strains induced by the ultrasonic transducers, this is a reasonable assumption. These sound speed values are comparable, but slightly higher than those found by Millett et al. for an unspecified grade of PEEK, $C_l = 2470 \pm 30$ and $C_s = 1060 \pm 30\ \mathrm{m\,s^{-1}}$ [22].

3.6. Fracture toughness measurements

Fracture toughness measurements were performed using compact tension (1/2CT, i.e., the specimen thickness b is half the specimen width w) specimens as previously presented by Brown and Dattelbaum [52]. The test geometry, as defined in ASTM Standard E-1820-01, is modified to enable a crack opening displacement (COD) gauge to be mounted along the loading line. The specimen notch was cut to have an inclusive angle of 40°, which was subsequently sharpened with a razor blade according to ASTM D5045. Tests were performed using a MTS 880 load frame under constant crosshead displacement rates of $0.025\ \mathrm{mm\,s^{-1}}$. Load–line displacements were measured with a MTS COD gauge 632.03E-31. Tests were performed at −50, 23, 100, and 150 °C using an MTS 612 environmental chamber. J-integral values corresponding to the ith data pair are given by:

$$J_i = J_{el} + J_{pl} = \frac{K_i^2(1-\nu^2)}{E} + \frac{\eta_{pl}A_i^{pl}}{b(w-a_0)} \tag{5}$$

where J_{el} and J_{pl} signify the division of energy into recoverable elastic deformation and permanent plastic deformation, respectively. The linear-elastic stress-intensity factor K_i for a specimen with a crack length of a_i is calculated according to ASTM Standard E-1820-01. The Poisson's ratio, ν, is taken to be 0.38, E is the Young's modulus, $\eta_{pl} = 2 + 0.522(w - a_{bi})/w$ is a dimensionless constant ($a_{bi} = a_0 + J_i/2\sigma_{ys}$ is the blunting corrected crack length corresponding to the ith data point), A_i^{pl} is the area under the load–displacement curve, and a_0 is the initial crack length. The width, w, and the thickness, b, of the specimen are nominally 39.8 and 19.1 mm, respectively. The initial tangent moduli and 2% offset yield stress values used in this work are given in Table 2. For unstable brittle fracture, as observed in PEEK below T_g, the peak load (P_{max}) provides a rigorous critical fracture criterion, $J_i(P_i = P_{max}) = J_{IC}$. To rigorously evaluate J_{IC} during stable crack propagation as observed above T_g, J–R curve data are constructed with the critical fracture criterion, J_{IC}, defined as the fracture toughness of the material at fracture instability prior to the onset of significant stable tearing crack extension (the point of 0.2 mm of crack growth beyond crack-tip blunting) through the normalization technique. The normalization technique was proposed by Landes and Herrera [53] and has been included in ASTM Standard E1820 for elastic–plastic fracture toughness. Although

Table 1
Ultrasonic wave-speeds and calculated isotropic elastic constants for PEEK at 23 °C

Material	C_l ($\mathrm{m\,s^{-1}}$)	C_s ($\mathrm{m\,s^{-1}}$)	E (GPa)	ν	G (GPa)	K (GPa)
PEEK 450G	2590 ± 10	1130 ± 10	4.6	0.38	1.7	6.6

Table 2
Mechanical properties for PEEK in tension as a function of temperature

Temperature (°C)	Tangent modulus (GPa)	2% Yield stress (MPa)
150	2.99	42.1
100	3.88	76.3
23	4.10	107.1
−50	4.28	141.3

[3] Panametrics 5077PR Pulser/Receiver, Panametrics V155 and V109 transducers. Timing obtained from a Tektronix TDS 754D Oscilloscope.

developed for metals, the normalization technique has been demonstrated to yield equivalent results to multi-specimen methods for a variety of polymers [54–56]. This method, as presented in full by Brown and Dattelbaum [52], uses an analytical solution with power law behavior for blunting and initiation, and smoothly transitions to a linear relationship for steady-state crack growth thus giving an accurate estimate of the crack-tip position over the course of the test.

3.7. Scanning electron microscopy

Fracture surface morphologies were examined with a JEOL JSM-6300FXV scanning electron microscope (SEM). After fracture, specimens were notched along the centerline from the backside and subsequently immersed in liquid nitrogen for approximately 30 min. Samples were immediately reloaded to propagate a brittle crack from the arrested crack tip. Areas of interests were then dissected, mounted, and sputtered with carbon to promote electrical conductivity to reduce charging. Micrographs were obtained using 5 keV secondary electrons.

3.8. Density measurements

A Micromeretics AccyPyc 1330TC helium pycnometer was used to measure density. The instrument has interchangeable 10, 3 and 1 cc sample cups and the smallest that would contain the specimen was used. Sample cup calibrations were verified against tungsten carbide reference spheres. Automated repeat runs were made until five sequential sample volume measurements had a standard deviation less than that of 0.02% of the nominal sample cup volume. Density was calculated from the sample mass and the average volume from the last five runs.

3.9. Taylor impact

Taylor cylinders were machined from the plate with dimensions of 7.62 mm in diameter by 38.1 mm long. Rods were fired at velocities between 150 and 360 m s^{-1} and temperatures of 23 and 100 °C. An Imacon 200 high-speed framing camera coupled to a Cordin 463 proportional delay generator was used to record back-lit images of the impacts. In all cases a 350 ns exposure was used and 16 frames were recorded with 15 μs inter-frame time. The system has been more fully described elsewhere [46]. Recovered specimens were potted in epoxy prior to polishing in the same manner as the hardness specimens.

4. Results and discussion

4.1. Compression and tension, 10^{-4}–10^{3} s^{-1}

Figs. 2 and 3 show the compressive response of the PEEK billet at various true strain rates and temperatures, respectively. It may be seen that over seven decades of strain-rate change, the yield strength increases by 30% from 128 to 184 MPa. Additionally, both plots show little or no strain

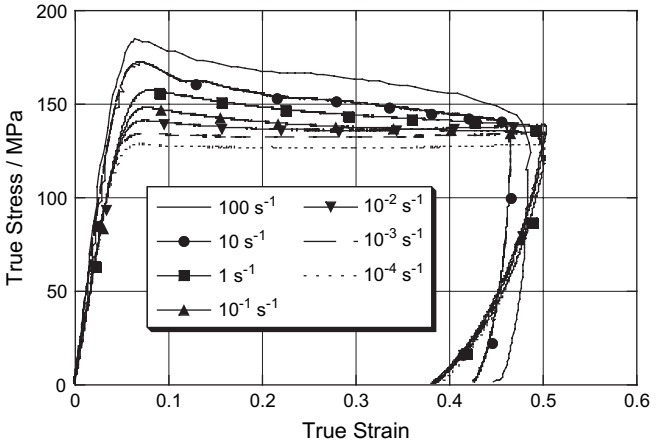

Fig. 2. Effect of strain rate on compressive properties of PEEK at 23 °C.

hardening, indeed at higher rates ($\geq 1 \times 10^{-2}$ s^{-1}) and the −85 °C test show strain softening. The temperature tests show a monotonic reduction in yield stress with increasing temperature. At 200 °C, well above the glass transition temperature ($T_g = 143$ °C), the samples exhibited no obvious yield point unlike specimens at lower temperatures. It may also be observed that the sample at 150 °C shows a very similar response to 140 °C suggesting that the T_g measured by DSC is slightly different from that found from mechanical techniques [57]. This is not too surprising since T_g is over a range that is frequency (or strain rate) dependent.

The compressive response at a strain rate of 3000 ± 200 s^{-1} is shown in Fig. 4 as a function of temperature. It may be seen that at all temperatures the material appears to strain soften. This effect was also seen in the higher rate quasi-static tests. The first part of each curve has been removed since the specimen was not in dynamic stress equilibrium at low strains.

Figs. 5 and 6 show the tensile response of the material. In all cases a distinct yield point is observed that represents the onset of necking, examples of which are shown in Fig. 7. This point also represents the breakdown in uniaxial stress.

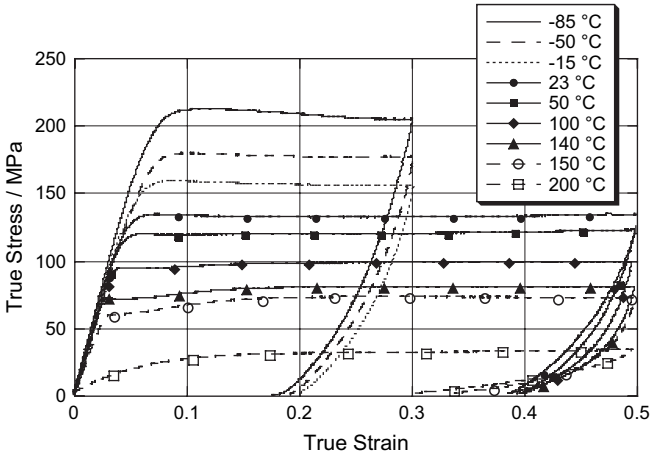

Fig. 3. Effect of temperature on compressive properties of PEEK at 1×10^{-3} s^{-1}.

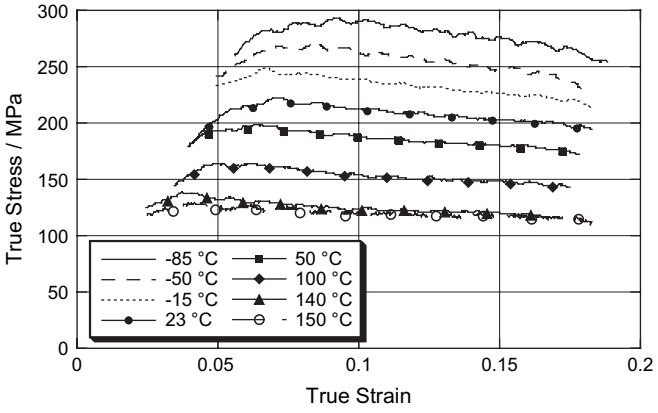

Fig. 4. Hopkinson bar compressive properties as a function of temperature. Strain rate = 3000 ± 200 s^{-1}.

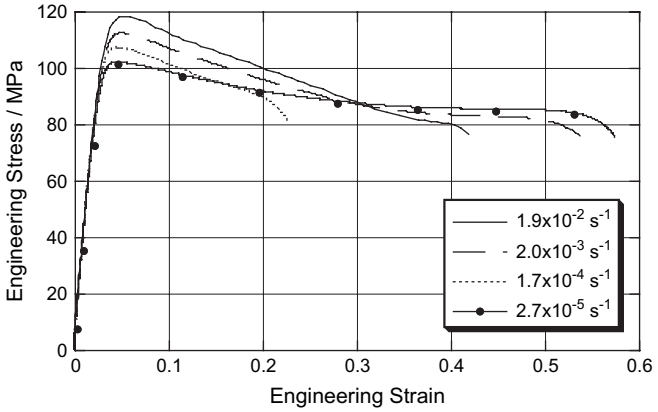

Fig. 5. Effect of strain rate on tensile properties at 23 °C.

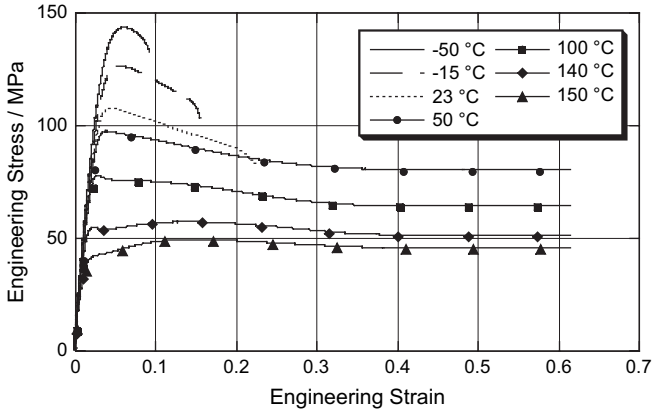

Fig. 6. Effect of temperature on tensile properties at a strain rate of 1.7×10^{-4} s^{-1}.

The engineering strain to failure shows no clear relationship in the case of the strain-rate experiments (i.e., there is no monotonic relationship). However, there is a clear upward trend in strain to failure when the temperature was increased. At temperatures of 100 °C and above, the travel on the extensometer was not large enough to follow the neck to failure. This was not thought to be important given the complex stress state existing at this stage. It may be seen from Fig. 5 that increasing

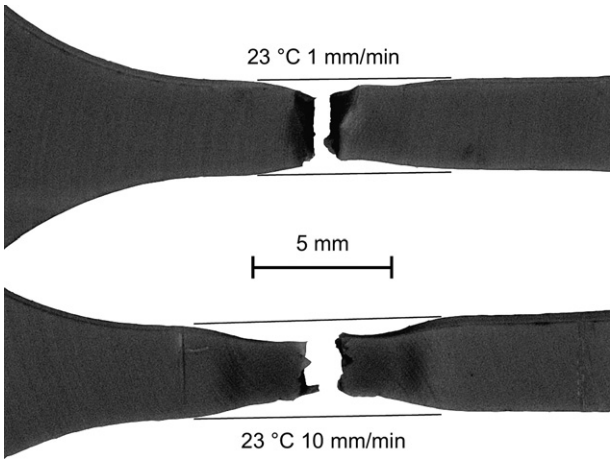

Fig. 7. Necking formation and failure in PEEK under tension.

the strain rate increases the yield stress and from Fig. 6 that increasing the temperature lowers it. It can be seen that the loading modulus up to yield seems unaffected by either the strain rate or temperature.

The variation in yield strength with temperature is shown in Fig. 8 for both tension and compression. It may be seen that the trend is generally linear over the studied temperature range with a suggestion of a non-linearity occurring at around T_g in both tension and compression. Additionally, the yield stress is lower in tension than in compression. Fig. 9 plots the variation in yield stress with changes in strain rate. As with temperature, the tensile yield stress is lower than the compression value but the gradient is similar between the two. The compressive yield stresses can be fit with a bilinear line although a smooth curve might work almost as well over the eight decades of strain rates studied. The intersection of the lines that fit to our data at a strain rate of ≈5 contradicts with the previous findings in PEEK 150G [17] where plots at four widely differing rates indicated a significant jump at strain rates above 5×10^2 s^{-1}. Fig. 10 plots the relationship between Young's modulus and

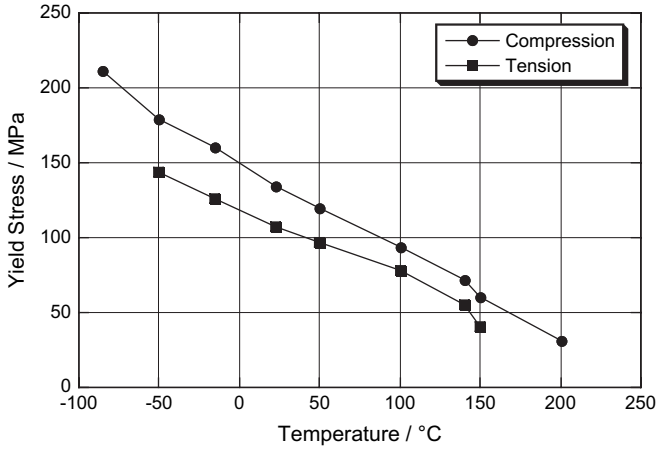

Fig. 8. The variation in yield stress with respect to temperature for tension and compression. Tensile strain-rate = 1.7×10^{-4} s^{-1}. Compressive strain-rate = 1×10^{-3} s^{-1}.

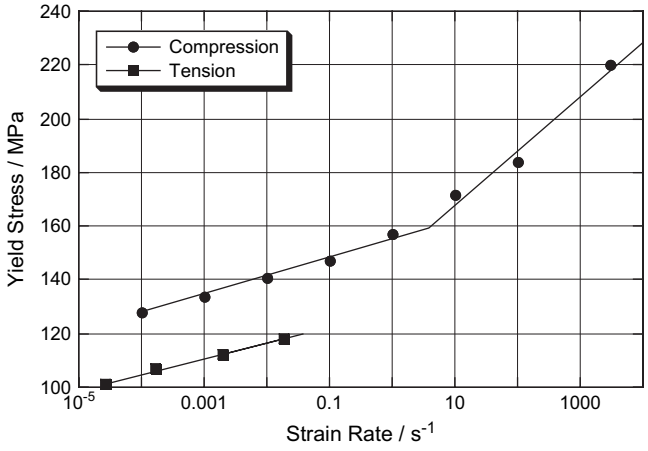

Fig. 9. The variation in yield stress with respect to strain rate in tension and compression at 23 °C.

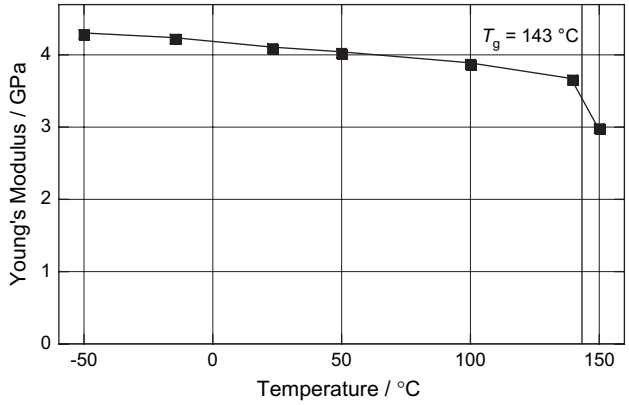

Fig. 10. The variation in Young's modulus with respect to temperature for tension. Strain rate = 1.7×10^{-4} s^{-1}.

temperature. While, as expected from DMA scans, the modulus only decreases slightly with temperature below the T_g, a significant decrease is observed just above T_g.

4.2. Taylor impact, $\approx 10^4$ s^{-1}

Approximately 30 Taylor cylinders were fired at velocities between 150 and 360 m s^{-1} and at temperatures of 23 and 100 °C. No substantial differences were noted in the response of the material at the two temperatures that would not be expected from the lower yield strength at elevated temperatures. The rest of this paper therefore deals exclusively with the qualitative and quantitative differences due to impact velocity.

All of our Taylor specimens deformed in a ductile manner with no formation of fragments at any velocity studied, this is consistent with a previous study by Millett et al. [47] who only obtained fragmentation at higher velocities than that reported here. At low velocities (150–250 m s^{-1}) a classic three diameter deformation pattern was noticed with the largest residual strains at the impact face while the back of the projectile remains undeformed. The specimen end remained reasonably flat and no cracking was observed. At medium velocities, 250–315 m s^{-1}, more extensive deformation was found at the impact face with the onset of small radial cracks that arrested before material separation occurred. In this velocity range visco-elastic effects appear to retracted the centre of the sample back after impact and resulted in a concave rod end with the appearance of a solidified 'melt' pool, as seen in Fig. 11. At higher velocities, 315–360 m s^{-1}, tearing in the visco-elastic pullback zone is observed with increasing effect at higher velocities, Fig. 11. Interestingly, the radial cracking present at medium velocities is absent at higher ones.

At all velocities, darkening of the rod is noticed in the highly deformed regions. These observations are also consistent with those of Millett et al. Efforts were therefore made to understand the origin of the 'melt' pool and the darkening. It is easy to establish that it is implausible that PEEK reaches the melt temperature under the conditions imposed at these impact velocities. The melt temperature of PEEK is 342 °C at atmospheric pressure, rising to 400 °C under the application of a hydrostatic stress of 100 MPa [58]. Assuming a specific heat capacity for PEEK of $c_p = 2180$ J kg^{-1} °C^{-1} [59] (N.B. in polymers typically $c_p \approx c_v$), a perfectly plastic yield strength of $\sigma_y = 150$ MPa and a maximum strain of $\varepsilon = 3$ (a considerable over estimate) the temperature rise assuming 100% of the input energy is converted to heat is approximately 160 °C ($\Delta T = \sigma_y \varepsilon / c_p \rho$). Shock heating might give rise to a further rise of ca. 10 °C. Therefore the end state temperature from an initial one of 23 °C can conceivably be not more than 200 °C, well short of the required melt temperature. The end section exhibiting the 'melt' like appearance must therefore be a result of the visco-elastic pullback.

Fig. 12 clearly shows the concave rod end and the discolouration associated with the large-strain regions. Investigations

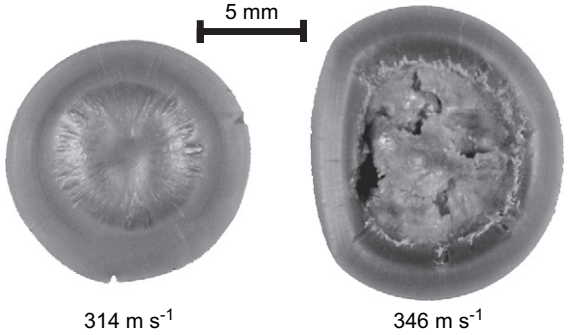

Fig. 11. End on view of two typical Taylor cylinders fired at 314 and 346 m s^{-1}. Starting temperature = 23 °C.

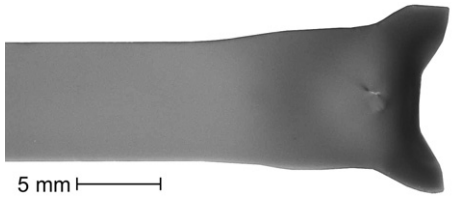

Fig. 12. Cross-section of a PEEK Taylor cylinder fired at 275 m s^{-1} and 100 °C. The colour change associated with the high-strain regions is obvious.

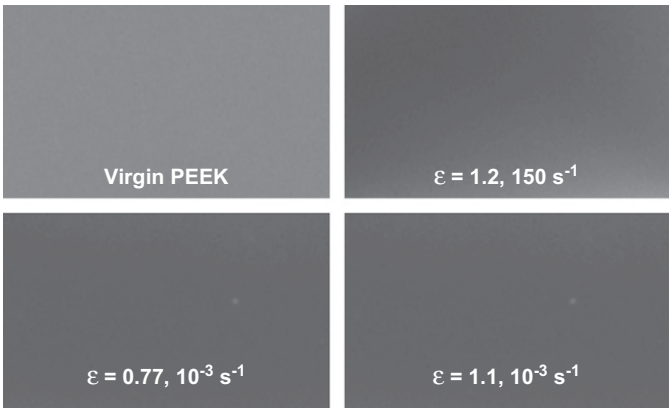

Fig. 13. Polished sections of four PEEK samples photographed under identical conditions to show the colour change associated with large-strain deformation. The grayscale value, in the range 0–255 where 255 is black, is 139 for virgin PEEK, 178 for $\varepsilon = 1.2$, 181 for $\varepsilon = 0.77$, and 181 for $\varepsilon = 1.1$.

were therefore focused to identify if the colour change was a result of the strain rate, strain or stress state. Fig. 13 shows a montage of cross-sections of virgin and three large-strain samples prepared and photographed under identical conditions. From the associated colour changes it is therefore clear that the colour change is associated with large-strain compression, not with strain rate. PEEK in tension undergoes stress whitening in common with many other polymers. Samples tested in compression to strains under ≈ 0.5 did not show significant colour change.

4.3. Large-strain compression

From Figs. 2 and 3 it may be seen that at modest strains (20–40%) in compression PEEK has an almost constant flow stress at quasi-static rates. Tests were done to see if under much larger strains the material starts to work harden. Fig. 14 shows two representative curves. In one case a right cylinder of 6.35 mm in diameter by 6.35 mm tall was loaded in a single deformation to large strains. Despite careful lubrication on highly polished WC platens, there can be no doubt that the result was affected by friction at larger strains. In an effort to remove this artifact and see if the hardening behavior is real, a similar sized sample was incrementally loaded with re-machining and lubrication between cycles. No sample barreling was observed at any stage on the incremental loading yet the work hardening rate seems higher than the friction affected sample. This behavior is not fully understood but may involve cold crystallization taking place between loadings. In any event it seems that PEEK does work harden at large strains under quasi-static compressive loading.

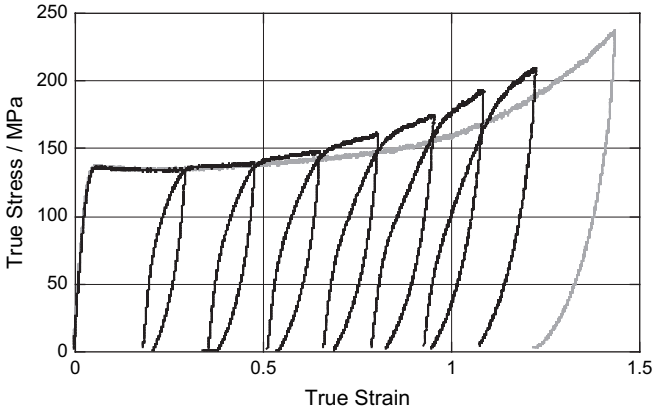

Fig. 14. Large-strain compression plot for PEEK showing the response to a single and incremental loading at 23 °C. Strain rate $= 1 \times 10^{-3}\ s^{-1}$.

To study the crystallinity of samples deformed to large strains at various temperatures, samples were deformed at a strain rate of $1 \times 10^{-3}\ s^{-1}$. Fig. 15 shows the resulting stress–strain curves. It may be seen that the −50 °C curve shows an upward trend from a strain of 0.4 matching the gradient of the sample deformed at 22 °C. The sample tested at 150 °C continues to show slight strain softening.

Vickers hardness measurements were made on various deformed PEEK samples to see the effect of large strains and associated discolouration. Fig. 16 shows measurements on a sectioned Taylor cylinder and a sample tested in a drop weight at a strain rate of $\approx 150\ s^{-1}$. In both cases it is clear that material subjected to large strains is softer than undeformed material. For reference, virgin PEEK samples had a hardness of $25.0 \pm 0.6\ kg\ mm^{-2}$ under the same conditions. The hardness measurements were approximately perpendicular to the loading axis, therefore a quasi-statically loaded sample was

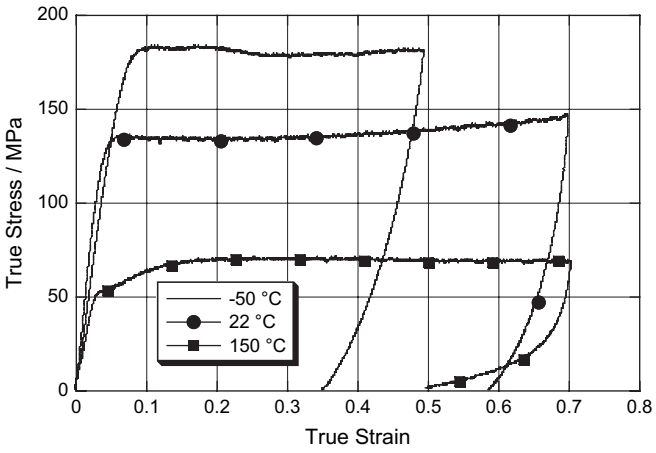

Fig. 15. Large compressive strain response of PEEK at three temperatures. Strain rate $= 1 \times 10^{-3}\ s^{-1}$.

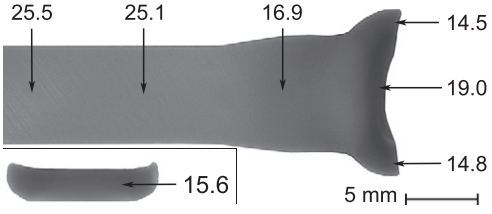

Fig. 16. Polished section of a typical Taylor sample showing the measured Vickers hardness values ($kg\ mm^{-2}$) at various points. Below is a cross-section of a small cylinder drop-weight deformed at $150\ s^{-1}$ to a strain of $\varepsilon = 1.1$ with a corresponding hardness measurement.

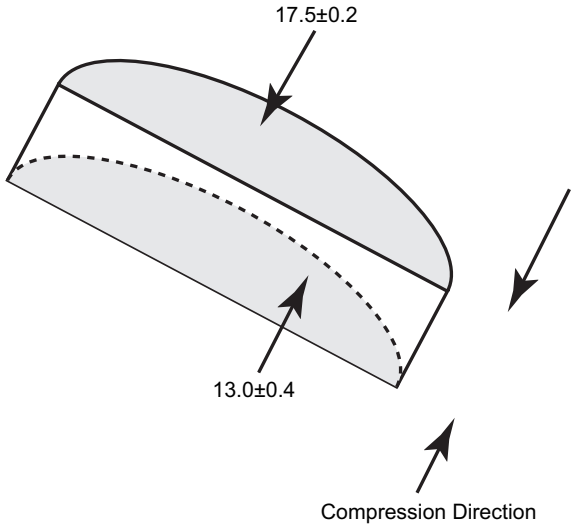

Fig. 17. Orthogonal hardness measurements (kg mm^{-2}) on an incrementally loaded cylinder, 1×10^{-3} s^{-1}, 23 °C, $\varepsilon_{residual} = 1.07$.

sectioned into two orthogonal directions to see if the material appeared oriented, Fig. 17. While the hardness value along the loading axis is higher than the perpendicular axis, each measurement is considerably softer than undeformed PEEK.

Samples of PEEK deformed at various temperatures and under differing conditions were tested to see if the molecular weight of the polymer was influenced, see Table 3. It was postulated that this may result in both the observed colour change and softening. Statistically, no difference was observed between samples, removing the possibility of chain scission as a method of polymer softening at high strain rates.

In an effort to understand the colour change associated with large-strain compression, a sample of PEEK was heated to 365 °C for 15 min before being quenched in ice water. The heating point was chosen to be well above the melting peak of 340 °C established from DSC experiments, but below the onset of thermal decomposition. The resulting crystallinity was found to be 31 ± 2%, this is higher than that might be expected for rapid quenching but results from the size of the sample used so that the glassy skin area could be excluded. Fig. 18 shows the colour after polishing this quenched material (a) in comparison to the as received material (b) when prepared and photographed under identical conditions. Clearly the lower crystallinity material (31 ± 2%) is darker than the as received PEEK (41 ± 2%). Hardness measurements were

Table 3
Inherent viscosity of various PEEK samples dissolved in concentrated (99%) sulphuric acid as a measure of molecular weight

Material	Inherent viscosity (dL g^{-1})
Virgin PEEK 450G	0.88 ± 0.02
Taylor impact zone, 23 °C at 311 m s^{-1}	0.89 ± 0.02
Taylor impact zone, 23 °C at 346 m s^{-1}	0.87 ± 0.02
Taylor impact zone, 100 °C at 347 m s^{-1}	0.90 ± 0.02
Hopkinson sample, 23 °C at 3000 s^{-1}	0.88 ± 0.02

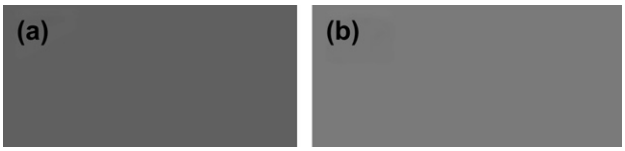

Fig. 18. The change in colour of PEEK with respect to crystallinity: (a) 31% water quenched from melt, (b) 41% as received PEEK 450G. The grayscale value, in the range 0–255 where 255 is black, is 163 for (a) and 135 for (b).

made on this sample and produced an average value of 22.7 ± 0.6 kg mm^{-2}, this is lower than the 25.0 ± 0.6 kg mm^{-2} value obtained for as received material.

Table 4 shows DSC crystallinity and density measurements on compression samples deformed to maximum strains of 0.7 and 1.0 at room temperature. The crystallinity clearly drops after testing in conjunction with the density. The crystallinity of semi-crystalline polymers is often measured using density from the assumption that amorphous material is less dense that fully crystalline and that there is a linear relationship between the two extreme states. The density values were used to estimate the mass fraction crystallinity (χ_c) using the following relation:

$$\chi_c = \frac{\rho_c(\rho - \rho_a)}{\rho(\rho_c - \rho_a)} \tag{6}$$

where ρ is the sample density, ρ_a is the extrapolated density of the pure amorphous phase (≈ 1260 kg m^{-3}) and ρ_c is the extrapolated density of the pure crystalline phase (≈ 1400 kg m^{-3}) [10].

The density determined crystallinity change is greater than the DSC one. This may be attributed to the fact that the DSC melt endotherm is affected by any polymer chain order while the density method assumes only a linear relationship between amorphous and fully crystalline states and ignores what form the material is in. It is reasonable to assume that large-strain compression introduced some measure of orientation into the polymer chains while apparently breaking up crystallinity. The resulting competing effects could therefore account for the smaller change in DSC measured crystallinity than that suggested from density.

The deformed ends of some Taylor specimens were removed to establish what effect impact velocity had on

Table 4
DSC measurements of residual crystallinity and density after compressive deformation to large strains

Material	DSC crystallinity (%)	Density (kg m^{-3})	Density crystallinity (%)
Virgin PEEK 450G	41 ± 2	1311 ± 1	39 ± 2
$\varepsilon_{max} = 0.7$ (1×10^{-3} s^{-1}) at 23 °C	34 ± 2	1294 ± 1	26 ± 2
$\varepsilon_{max} = 1.0$ (1×10^{-3} s^{-1}) at 23 °C	32 ± 2	1287 ± 1	21 ± 2
$\varepsilon_{max} = 0.5$ (1×10^{-3} s^{-1}) at −50 °C	38 ± 2	1307 ± 1	36 ± 2
$\varepsilon_{max} = 0.5$ (1×10^{-3} s^{-1}) at 150 °C	40 ± 2	1304 ± 1	33 ± 2
$\varepsilon_{max} = 0.7$ (1×10^{-3} s^{-1}) at 150 °C	39 ± 2	1296 ± 1	28 ± 2

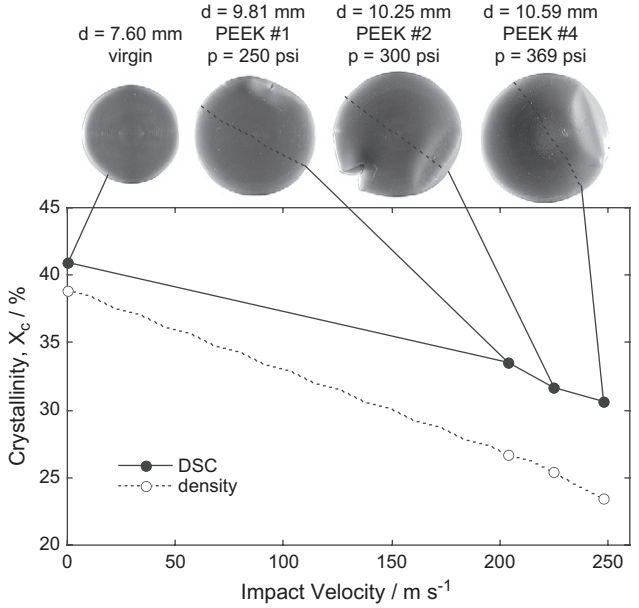

Fig. 19. The change in crystallinity at the ends of the PEEK Taylor samples as a function of impact velocity measured by DSC and density techniques.

crystallinity. Fig. 19 shows the effects of impact velocity on percentage crystallinity measured by DSC and density techniques. Clearly increasing the impact velocity lowers the crystallinity measured by both methods but the change by density is greater. The figure also reports the diameter at the ends of the rods. As expected, increasing the velocity results in greater residual strain.

4.4. DSC

DSC scans at 10 °C min^{-1} were undertaken on specimens deformed at low and high strain rates. Fig. 20 shows the scans of four samples compressed to differing true strains and Fig. 21 shows the scans from the ends of four room temperature Taylor samples impacted at differing velocities. In each

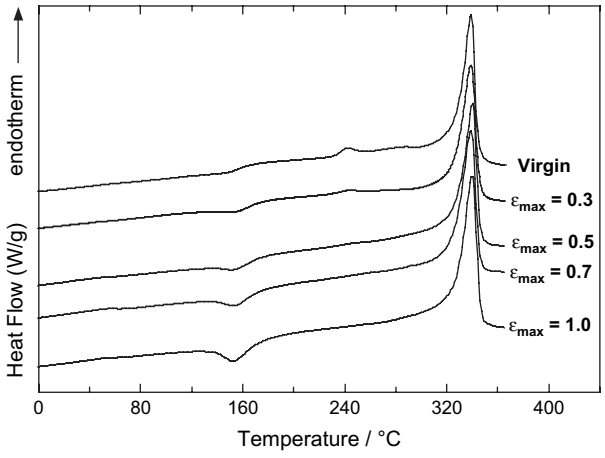

Fig. 20. DSC scans of compression cylinders deformed to differing maximum true strain (1×10^{-3} s^{-1} at 22 °C).

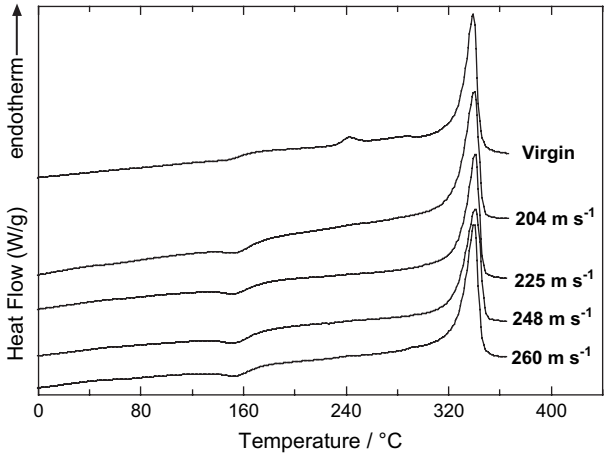

Fig. 21. DSC scans of the ends of room temperature Taylor cylinders fired at differing velocities.

case, the DSC scans of virgin PEEK show a T_g of 158 °C and a broad melting endotherm. The melting endotherms display a small peak at 242 °C with the predominant melting peak at 341 °C. Upon deformation, by either Taylor impact or quasi-static compression, the peak at 242 °C disappears suggesting some disruption in the crystal structure. Furthermore, the region around T_g develops an exotherm. This exothermic behavior increases with increasing deformation. The exothermic behavior may be due to non-equilibrium order imposed in the material by deformation. The ordered structure was then frozen by the high T_g and upon heating above T_g, the chains have sufficient mobility to anneal out the order. In both Figs. 20 and 21, the melting temperature is seen to increase by 2–3 °C with increasing deformation.

4.5. Fracture

Fracture experiments were performed at −50, 23, 100, and 150 °C. Quasi-static (0.025 mm s^{-1}) load–displacement curves for PEEK are shown in Fig. 22. Below T_g, the load

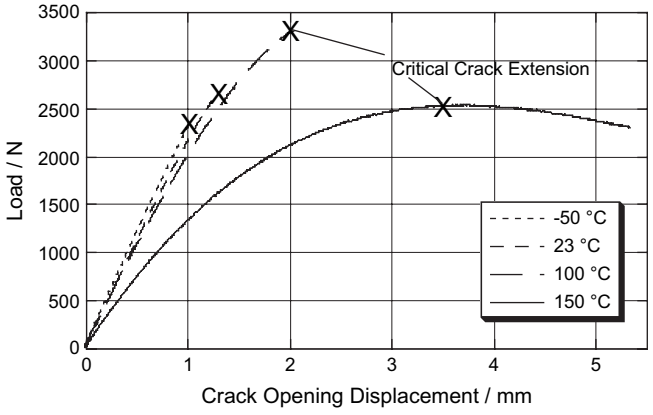

Fig. 22. Representative load–displacement curves as a function of temperature at a displacement rate of 0.025 mm s^{-1}. The critical crack extension markers indicate the point of catastrophic crack propagation below T_g, and stable crack growth based on J–R curve data above T_g.

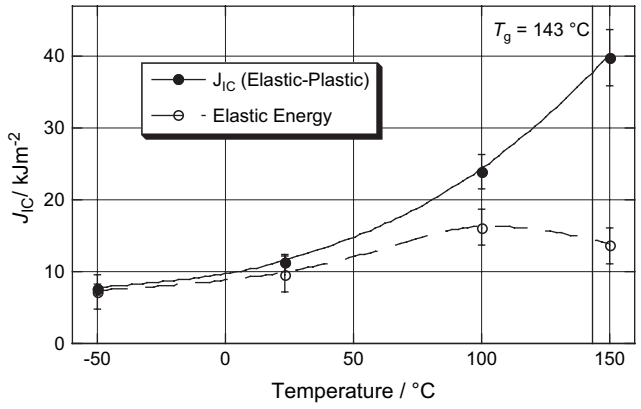

Fig. 23. Fracture toughness values, J_{IC}, as a function of temperature and elastic partition from LEFM G_{IC} analysis.

increases with crack opening displacement δ to a maximum load P_{max} at which point the crack catastrophically propagates through the specimen. Increasing temperature leads to a higher peak load and an increasing degree of non-linearity in the $P-\delta$ response. The catastrophic onset of crack growth allows for the peak load to be used as the critical crack extension criterion. The resulting critical energies from both the full elastic–plastic analysis in the form of the J_{IC} and the elastic portion representative of a linear-elastic G_{IC} analysis (or the elastic portion of Eq. (5)) are plotted in Fig. 23. Fracture surfaces are shown in Fig. 24. While at −50 °C the crack propagated nominally along the centerline of the CT specimen, at 23 and 100 °C the crack bifurcated after propagating a short distance. At room temperature and below, the contribution from the plastic portion of Eq. (5) is within the error of the linear-elastic measurement. At 100 °C the plastic contribution is no longer negligible, representing nearly one-third of the energy in the sample. Above T_g, the load increase exhibits strong non-linearity asymptoting to a peak load P_{max} followed by stable declining load. Both the $P-\delta$ profile and observation of the sample exhibit stable–ductile elastic–plastic crack propagation behavior. The $J-R$ behavior of PEEK above T_g is illustrated in Fig. 25. The critical crack extension based on a 0.02 mm extension beyond crack-tip blunting, indicated in Fig. 22, corresponds to a load level P_C at 99.5% of P_{max}. While below T_g both the elastic and plastic contributions increase with temperature (Fig. 23), above T_g the elastic portion diminishes and over 65% of J_{IC} strain energy comes from the plastic partition.

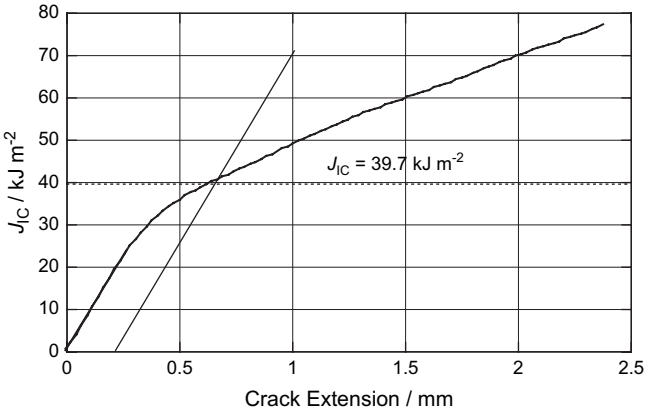

Fig. 25. Representative $J-R$ curve as a function for PEEK at 150 °C obtained using the normalization technique.

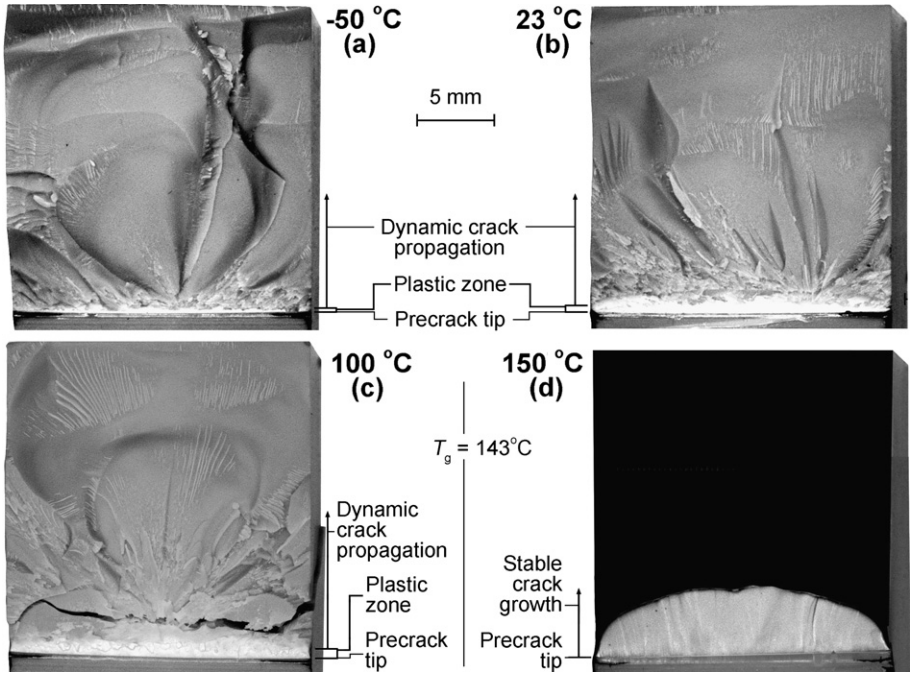

Fig. 24. Optical micrographs of the fracture plane morphology for PEEK as a function of temperature at 0.025 mm s^{-1} loading rate. Note: crack propagation is from bottom to top.

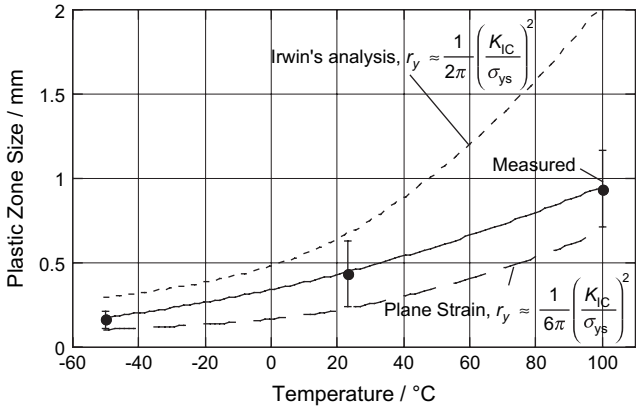

Fig. 26. Measured and LEFM approximation of plastic zone size as a function of temperature.

Below T_g, fracture surfaces of PEEK exhibit two distinct zones. As indicated in Fig. 24, a distinct plastic zone is present at the location of the precrack tip. Plastic zone sizes from 9-point averages for the three temperatures investigated are plotted in Fig. 26. Theoretical estimates for the plastic zone size based on LEFM are plotted using the material properties given in Tables 2 and 5. Despite neglecting the plastic energy absorbed by the material, applying the elastic portion reasonably captures the plastic zone size. The plane strain solution slightly underestimates the plastic zone size, most likely due to disregarding the plastic behavior, while Irwin's analysis [20] based on the plane stress condition provides an upper bound. Beyond the plastic zone, the fracture surface is largely brittle with isolated regions of river markings.

5. Discussion and conclusions

PEEK 450G exhibits the usual sensitivity to both temperature and strain rate in tension and compression found in many semi-crystalline polymers. The loading modulus is largely unaffected by either strain rate or temperature below the glass transition temperature. In tension, the room temperature quasi-static Young's modulus was measured as 4.1 GPa compared with 4.6 GPa from the ultrasonic tests at a similar temperature. The difference can be explained by the minute strain imposed by ultrasonic deformation requiring almost no polymer chain sliding and a small effect from the higher strain-rate. The plot of flow stress versus strain rate (Fig. 9) can be fit by a bilinear relationship as suggested by Hamdan and Swallowe [17–19] but the intersection is at a strain rate of ≈ 5 which is an order of magnitude lower than that reported previously. It is unclear if this discrepancy is due to the different material grades tested (150G rather than 450G), the differing testing methods or the increased number of compressive rates reported in this report. At modest strains ($\varepsilon < 0.7$) and under most conditions, PEEK seems to have either an approximately constant or decreasing flow stress. It has been shown that at large strains ($\varepsilon > 1.0$), room temperature and quasi-static strain rates, PEEK begins work hardening.

Table 5
Comparison of the J_{IC} solution to the LEFM K_{IC} solution with respect to temperature

Temperature (°C)	G_{IC} (kJ m^{-2})	ν	K_{IC} (MPa m$^{1/2}$)	Error[a] (%)
−50	7.19	0.38	6.00	6
23	9.66	0.38	6.87	14
100	16.21	0.38	8.58	32

[a] Error captures the degree to which the LEFM solution for K_{IC} neglects the non-linear behavior of PEEK, defined as $(J_{IC} - K_{IC})/J_{IC}$.

In the research reported here, the crystallinity of all samples deformed to large strains was found to decrease. This differs from the work of Hamdan and Swallowe [17–19] who reported increase in crystallinity of samples deformed to large strains under adiabatic conditions, especially when the initial sample starting temperature was above T_g. In a later paper, Swallowe and Fernandez studied another semi-crystalline polymer, PET, and again showed an increase in crystallinity when deformed adiabatically to large strains or when deformed at high temperature [60]. This later research also showed that the crystallinity increase occurred predominately after the test was complete, but before the sample had cooled below the crystallization temperature. Therefore the increase in crystallinity measured after the test could not be responsible for the increase in flow stress seen under some rapid adiabatic deformation conditions. In our research, deformations to strains above 0.7 mostly occurred from samples starting at room temperature. In this case, the temperature rise associated with even the large strains seen in the Taylor test would not be sufficient to heat the sample to a temperature at which rapid crystallization would occur (ca. 260 °C). From the research of Hamdan and Swallowe it might be expected that an increase in crystallinity would be seen in samples deformed adiabatically to very large strains (≈ 1.4), or from starting temperatures around 200 °C.

The results of the Taylor impact experiments are fully consistent with those reported by Millett et al. [47] in terms of the deformation modes with respect to velocity and the observed browning of the rod ends. Vickers hardness tests on the sectioned rods showed a significant lowering in hardness in the highly deformed zones. This seems at odds with the observation that at large strains PEEK work hardens. An explanation for this is not obvious. It has been shown that the browning effect in PEEK observed initially in the Taylor impacts is a result of large compressive strain, independent of the strain rate. It has also been shown that large compressive strain lowers the crystallinity at both quasi-static and Taylor impact strain rates ($\approx 10^4$ s^{-1}). Consistent with these results is the softening found in the PEEK sample heat treated to obtain lower crystallinity compared with virgin material. Significantly, however, the Vickers hardness observed in undeformed material of lower crystallinity (31%) is 22.7 kg mm^{-2} compared with hardness values of 14.5–19 kg mm^{-2} found in deformed Taylor ends with a crystallinity of 31–33.5%. This implies that the drop in hardness cannot fully be explained by the crystallinity reduction alone and that compressive deformation also plays a role. Despite this, a consistent picture emerges relating to the Taylor samples; the high-speed impact imparts

large strains to the material that lower the crystallinity, this reduces the hardness and makes the material appear darker to the eye. The higher the impact speed, the larger the compressive strain and the lower the crystallinity measure in the deformed rod ends. Finally, the molecular weight of the material is unchanged after straining under any of the conditions reported here.

Fig. 27 compares the elastic–plastic and linear-elastic critical energy fracture toughness values from the current work with a range of values from the literature. As discussed earlier, with the exception of work from Hashemi [40] and Arkhireyeva and Hashemi [41] based on the EWF, all of the literature values were given as K_{IC} and have been recalculated as G_{IC} by the current authors. The vast majority of literature data is focused on the room temperature condition, which is expanded in the inset of Fig. 27. The literature values for the room temperature fracture toughness of PEEK show close agreement with the elastic portion from the current work lying in the middle of the literature values. Addition of the plastic contribution to full elastic–plastic *J*-integral fracture toughness places the fracture toughness above the mean of the literature values, albeit still within the scatter of published data. Below room temperature the current work remains in close agreement with that of Karger-Kocsis and Friedrich [29].

Above room temperature the elastic portion from the current work diverges from the Karger-Kocsis data, which is likely due to the difference in crystallinity of the PEEK in these two studies. While both studies investigated PEEK 450G, the material investigated by Karger-Kocsis and Friedrich had crystallinity of only 23.1 and 22.5% by DSC and density techniques, respectively, i.e., 17% lower than the current work. However, above room temperature the plastic contribution to J_{IC} increases in significance and becomes dominant above T_g. This greatly decreases the consequence of the difference in the elastic contribution between the current work and that of Karger-Kocsis and Friedrich. In the higher temperature regime, the measured J_{IC} values approach the EWF values of Hashemi and Arkhireyeva and Hashemi. In some ways this may be reasonable as above T_g the mechanism of crack propagation in PEEK could be convincingly described as necking and tearing, for which the EWF is proposed. This is opposed to the rapid-brittle fracture demonstrated by PEEK below the T_g, for which the EWF is not intended. Moreover, Hashemi and Arkhireyeva and Hashemi showed that the bulk yielding contribution to the EWF, which cannot be directly correlated to the classic linear-elastic fracture toughness, decreases with temperature making only a minor contribution above T_g. That being said, there is insufficient evidence to conclude that the similarity is not simply coincidence, especially as these EWF studies investigated non-pedigreed PEEK of unknown grade or crystallinity. Also, as

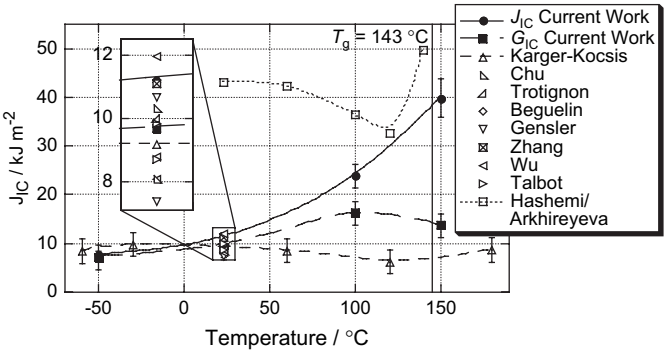

Fig. 27. Fracture toughness of PEEK from Fig. 23 compared with literature values.

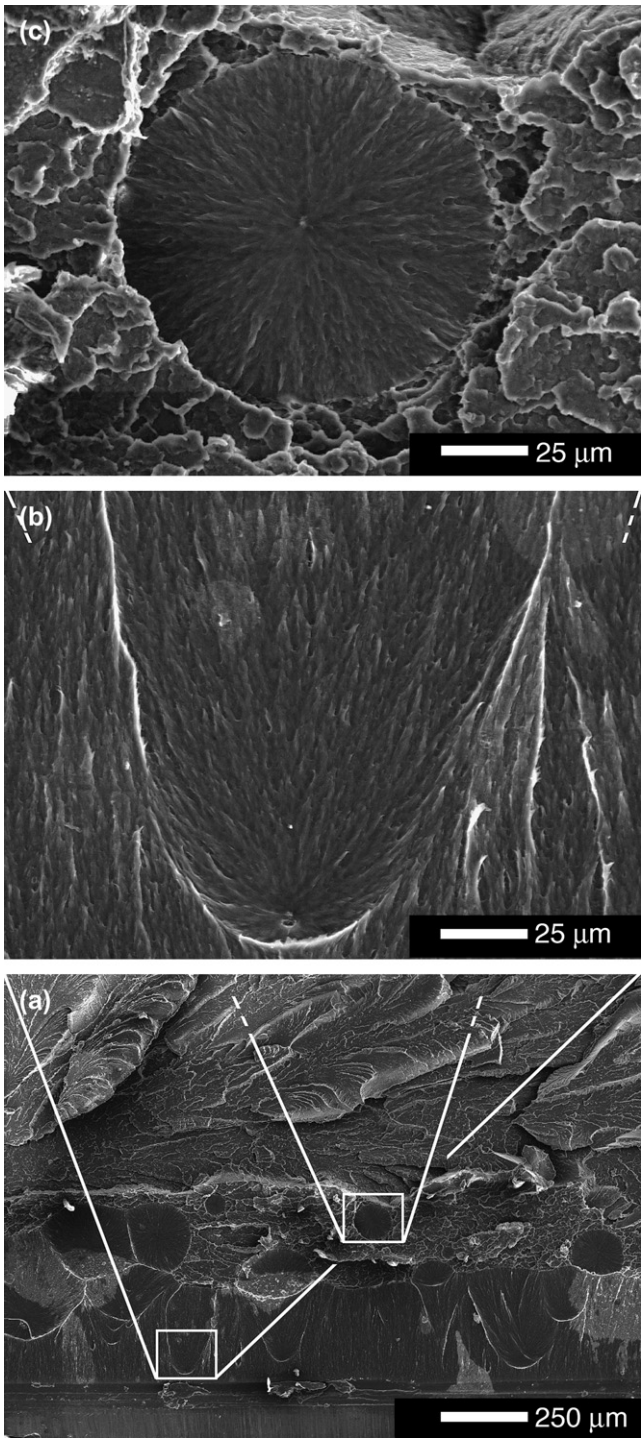

Fig. 28. SEM micrographs of PEEK plastic zone fracture plane morphology at 23 °C. Note: crack propagation is from bottom to top.

demonstrated by Zhao and Li [61] the EWF technique is extremely sensitive to thickness for PEEK in the range used by Hashemi [40] and Arkhireyeva and Hashemi [41]. This makes their results specimen specific rather than material properties.

Changes in the fracture mechanisms of PEEK associated with temperature were further elucidated by scanning electron microscopy investigation of the fracture plane morphology. The plastic zone observed by optical microscopy (Fig. 24) below the T_g consists of ductile flow in from the precrack tip with numerous radial slow-growth domains indicative of void nucleation and coalescence type failure processes (see Fig. 28a). In the region closest to the precrack tip the boundaries are primarily parabolic in shape, Fig. 28b. The preferential direction is that of ultimate crack growth, but more importantly demonstrates an evolution in the direction of the sweeping stress-intensity profile. At the interface between the plastic zone and the onset of fast fracture, nucleation sites are observed to exist beyond the continuous plastic zone. That is to say that previously nucleated parabolic features have not propagated to join with the stable propagation from these lone nucleation sites, but rather surrounded by fast fracture, shown in Fig. 28c. These sites are near perfect disks with uniform propagation in all directions. These parabolic features have previously been observed [29,30,32] in PEEK 450G in regions of high stress concentration, although not directly correlated to the crack-tip plastic zone. Interestingly, however, while Chu and Schultz [30] observed these fracture features to be present in PEEK 450G, they do not occur in the lower molecular weight PEEK 150P. Chu and Schultz proposed a mechanism

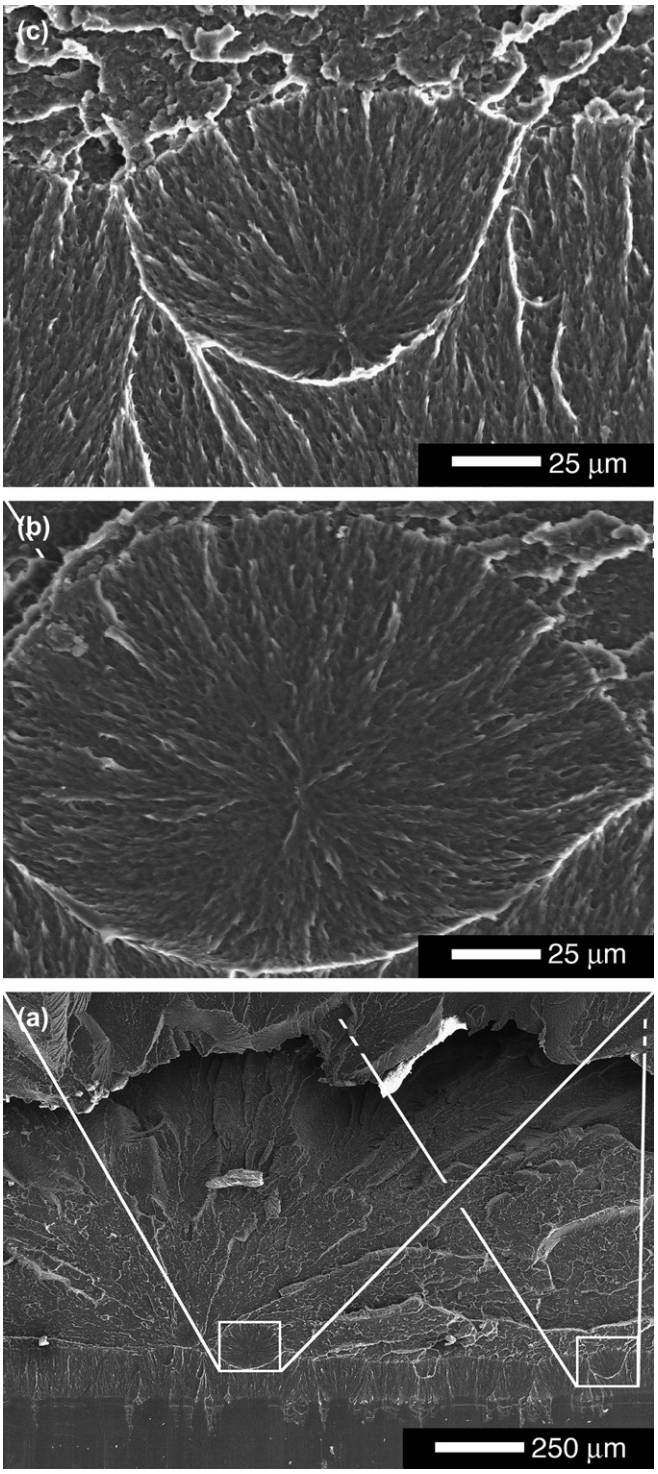

Fig. 29. SEM micrographs of PEEK plastic zone fracture plane morphology at −50 °C. Note: crack propagation is from bottom to top.

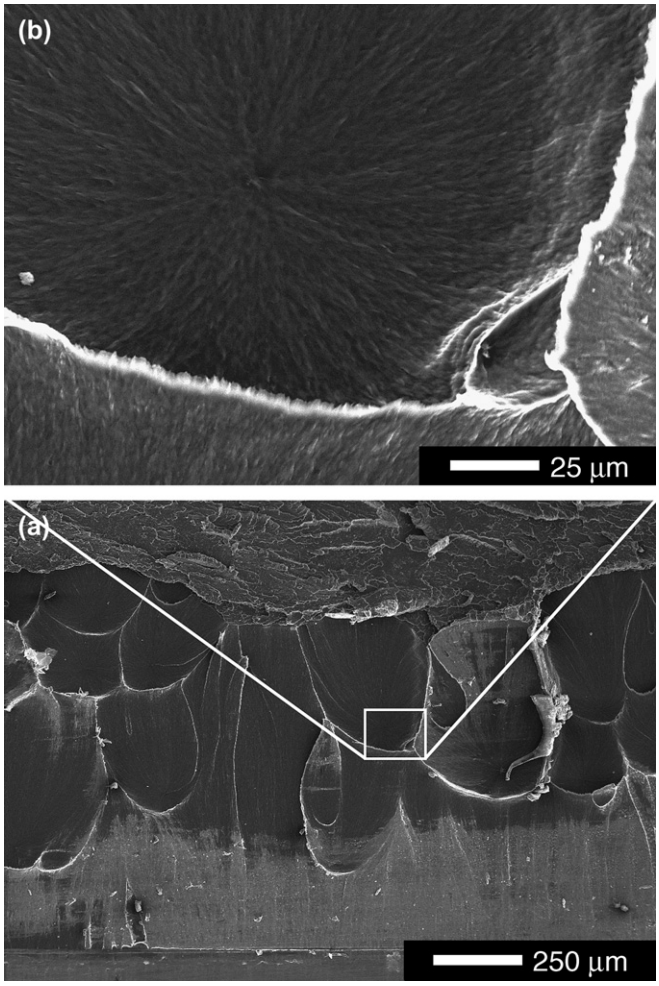

Fig. 30. SEM micrographs of PEEK plastic zone fracture plane morphology at 100 °C. Note: crack propagation is from bottom to top.

of defect-induced microcracks in the high stress concentration region near the crack tip due to the inclusion of impurities.

In the current work, close investigation of the nucleation sites failed to reveal a distribution of second phase impurities. The containment of these features to the region of yielded material and the drawn nature of the morphology suggest ductile deformation rather than stable crack growth per se. The failures initiated at randomly distributed weaker nucleation points and coalesced. The effect of temperature on the plastic zone morphology is illustrated in Fig. 29 and 30. Karger-Kocsis and Friedrich [29] reported his surprise at finding a relatively large plastic zone in front of the crack tip even at temperatures far below room temperature. As discussed earlier the size of the plastic zone size is as expected given the polymers' fracture toughness and yield stress. However, as seen in Fig. 29, the occurrence of nucleation ahead of the crack tip is substantially retarded by the decreased temperature. The majority of the plastic zone consists of ductile yielding propagating from the crack tip. It is worth noting that these features associated with deformation from nucleation points decrease substantially in size in the direction of crack growth and a lesser degree parallel to the precrack tip. Conversely, as seen in Fig. 30, increased temperature leads to larger parabolic features as well as more uniform nucleation.

Much less has been reported on fractography from the fast fracture regime. Karger-Kocsis and Friedrich reported characteristic veins or river markings representative of plastic flow. Moreover, they suggested that the density and thickness of veins increase qualitatively with temperature. Although Kemmish and Hay [39] made no comment of river markings, they are present in his micrographs. In the current work river markings are also a prominent feature in the fast fracture regime, as shown in Fig. 31. As illustrated from Fig. 31a, the density and thickness of river markings can have as much to do with location on the fracture plane as it does to do with variables such as loading rate or temperature. That said, the results of current work broadly agree with Karger-Kocsis and Friedrich observation. At decreased temperature, shown in Fig. 32, river markings are much more subtle and are completely absent in large areas (Fig. 32b). At increased temperatures, shown in Fig. 30, the river markings are much more distinctive and the overall morphology exhibits a greater

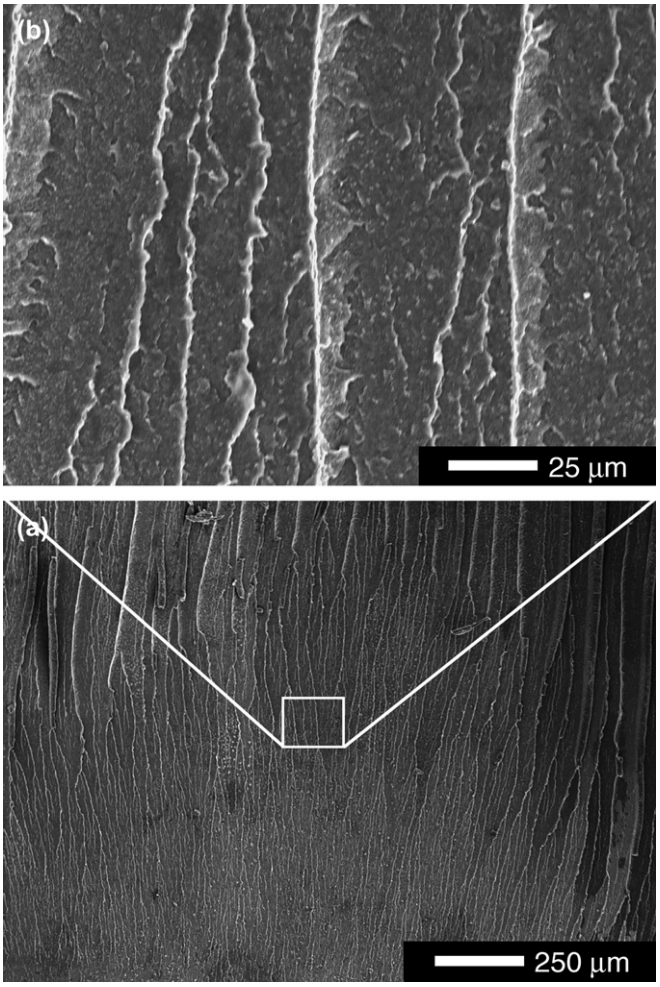

Fig. 31. SEM micrographs of PEEK brittle fracture plane morphology at 23 °C. Note: crack propagation is from bottom to top.

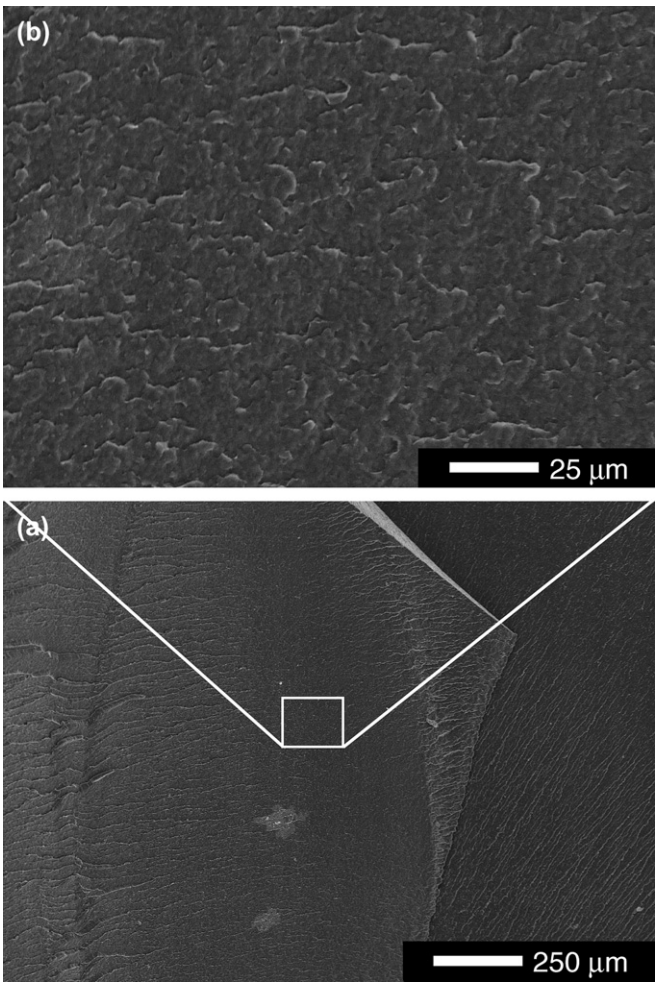

Fig. 32. SEM micrographs of PEEK brittle fracture plane morphology at −50 °C. Note: crack propagation is from bottom to top.

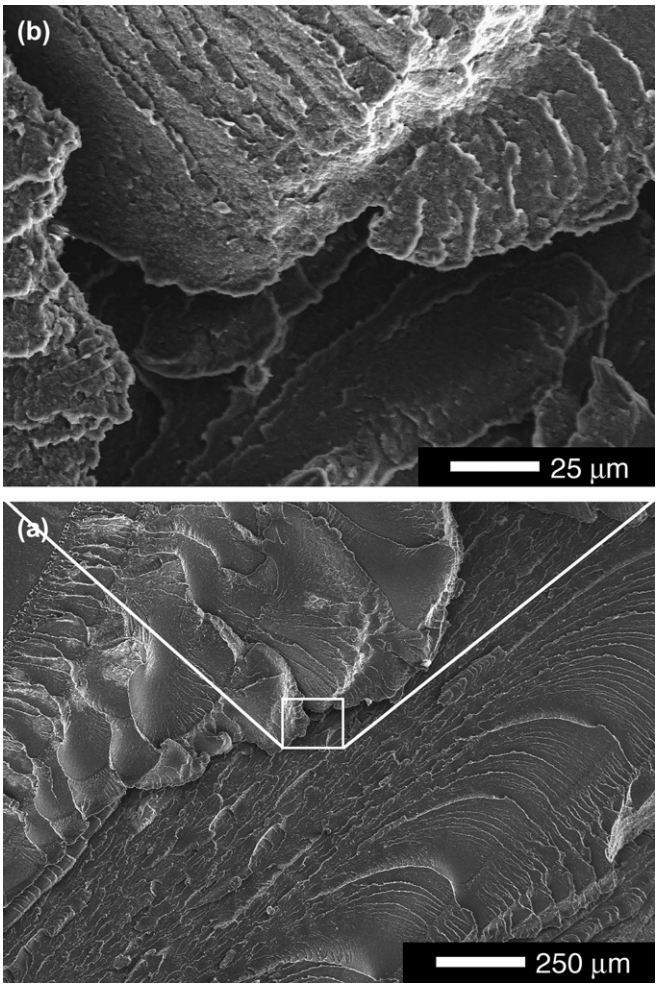

Fig. 33. SEM micrographs of PEEK brittle fracture plane morphology at 100 °C. Note: crack propagation is from bottom to top.

degree of micro-scale deformation (Fig. 33). Of interest the increasingly dramatic micro-scale features with temperature is contrary to the meso-scale fracture morphology, which actually becomes increasingly planar with temperature (see Fig. 24).

Above T_g, the fracture morphology offers much less of note, as shown in Fig. 34. There is no clear plastic zone (Fig. 34b) or noteworthy morphology in the region of constant crack growth rate (Fig. 34d). Moreover, the micro-scale morphology at the microscale (Fig. 34c and e) exhibits similarly drawn finger-like morphology. This structure is also very similar to the underlying structure observed below T_g in the plastic zone (Figs. 28b,c, 29b,c and 30b) and in the fast fracture regime (Figs. 31b and 32b). This suggests that at the length scale of the crystalline spherulite, there is a common fracture mode independent of temperature or deformation regime. Chu and Schultz [30] previously showed that the drawn finger-like morphology at this length scale to be representative of intraspherulitic fracture in 450G at room temperature, i.e., the crack prefers to propagate through the softer amorphous polymer rather than the harder and stronger crystalline domains. The current work shows intraspherulitic fracture to dominate in PEEK 450G over a much wider range of conditions.

Acknowledgements

The authors gratefully acknowledge financial support for this research from the joint DOD/DOE Office of Munitions Memorandum of Understanding project on the dynamic behavior of polymers. The research was performed under the auspices of the US Department of Energy. Dr. Lee Perry is thanked for help in using the LANL drop-weight apparatus.

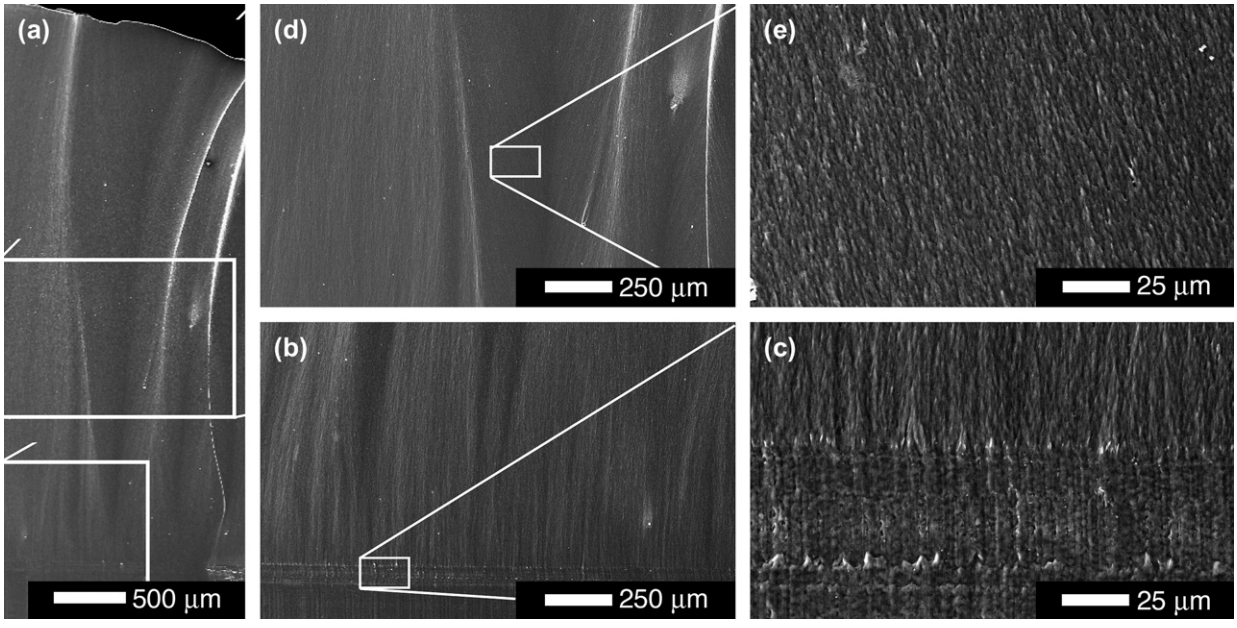

Fig. 34. (a) SEM micrographs of PEEK ductile fracture plane morphology above T_g at 150 °C in the region of (b,c) initial and (d,e) steady-state crack growth. Note: crack propagation is from bottom to top.

References

[1] Attwood TE, Dawson PC, Freeman JL, Hoy LRJ, Rose JB, Staniland PA. Synthesis and properties of polyaryletherketones. Polymer 1981;22: 1096–103.

[2] Jonas A, Legras R, Issi JP. Differential scanning calorimetry and infrared crystallinity determinations of poly(aryl ether ether ketone). Polymer 1991;32:3364–70.

[3] Sauer BB, Kambert WG, Neal-Blanchard E, Threefoot SA, Hsiao BS. Temperature modulated DSC studies of melting and recrystallization in polymers exhibiting multiple endotherms. Polymer 2000;41:1099–108.

[4] Wei CL, Chen M, Yu FF. Temperature modulated DSC and DSC studies on the origin of double melting peaks in poly(ether ether ketone). Polymer 2003;44:8185–93.

[5] Kong Y, Hay JN. The measurement of the crystallinity of polymers by DSC. Polymer 2002;43:3873–8.

[6] Blundell DJ, Osborn BN. The morphology of poly(aryl-ether-ether-ketone). Polymer 1983;24:953–8.

[7] Fratini AV, Cross EM, Whitaker RB, Adams WW. Refinement of the structure of PEEK fibre in and orthorhombic unit cell. Polymer 1986; 27:861–5.

[8] Wakelyn NT. Variation of the unit cell parameters of poly(arylene ether ether ketone) film with annealing temperature. J Polym Sci Polym Lett Ed 1987;25:25–8.

[9] Hay JN, Langford JI, Lloyd JR. Variation in unit cell parameters of aromatic polymers with crystallization temperature. Polymer 1989;30:489–93.

[10] Bas C, Grillet AC, Thimon F, Alberola ND. Crystallization kinetics of poly(aryl ether ether ketone): time–temperature-transformation and continous-cooling transformation diagrams. Eur Polym J 1995;31:911–21.

[11] Talbott MF, Springer GS, Berglund LA. The effects of crystallinity on the mechanical properties of PEEK polymer and graphite fiber reinforced PEEK. J Compos Mater 1987;21:1056–81.

[12] Lee LH, Vanselow JJ, Schneider NS. Effects of mechanical drawing on the structure and properties of PEEK. Polym Eng Sci 1988;28(3):181–7.

[13] Chivers RA, Moore DR. The effect of molecular weight and crystallinity on the mechanical properties of injection moulded poly(aryl-ether-ether-ketone) resin. Polymer 1994;35(1):110–6.

[14] Dahoun A, Aboulfaraj M, G'Sell C, Molinari A, Canova GR. Plastic behavior and deformation textures of poly(ether ether ketone) under uniaxial tension and shear. Polym Eng Sci 1995;35:317–30.

[15] Alberola ND, Mele P, Bas C. Tensile mechanical properties of PEEK films over a wide range of strain rates II. J Appl Polym Sci 1997; 64:1053–9.

[16] Cady CM, Blumenthal WR, Gray III GT, Idar DJ. Determining the constitutive response of polymeric materials as a function of temperature and strain rate. J Phys IV France 2003;110:27–32.

[17] Hamdan S, Swallowe GM. Crystallinity in PEEK and PEK after mechanical testing and its dependence on strain rate and temperature. J Polym Sci Part B Polym Phys 1996;34:699–705.

[18] Hamdan S, Swallowe GM. The strain-rate and temperature dependence of the mechanical properties of polyetherketone and polyetheretherketone. J Mater Sci 1996;31:1415–23.

[19] Swallowe GM, Fernandez JO, Hamdan S. Crystallinity increases in semi crystalline polymers during high rate testing. J Phys IV France 1997; 7:C3-453–9.

[20] Walley SM, Field JE, Pope PH, Safford NA. The rapid deformation behaviour of various polymers. J Phys III 1991;1(12):1889–925.

[21] Bas C, Alberola ND. Dynamic mechanical behavior of poly(aryl ether ether ketone) in the -150° to $+100^{\circ}$ temperature range: influence of the nature of sorbed solvents. Polym Eng Sci 1996;36:244–53.

[22] Millett JCF, Bourne NK, Gray III GT. The response of polyether ether ketone to one-dimensional loading. J Phys D Appl Phys 2004;37: 942–7.

[23] Millett JCF, Gray III GT, Bourne NK. Longitudinal and lateral stress measurements in shock loaded polyether ether ketone. AIP Conf Proc 2004;706(1):663–6.

[24] Donaldson SL. Fracture toughness testing of graphite/epoxy and graphite/peek composites. Composites 1985;16(2):103–12.

[25] Crick RA, Leach DC, Moore DR. Interpretation of toughness in aromatic polymer composites using a fracture mechanics approach. In: Thirty-first International SAMPE Symposium; April 7–10, 1986. p. 1677–89.

[26] Béguelin P, Barbezat M, Kausch HH. Mechanical characterization of polymers and composites with a servohydraulic high-speed tensile tester. J Phys III France 1991;1:1867–80.

[27] Fracasso R, Rink M, Pavan A, Frassine R. The effects of strain-rate and temperature on the interlaminar fracture toughness of interleaved PEEK/CF composites. Compos Sci Technol 2001;61:57–63.

[28] Jacob GC, Starbuck JM, Fellers JF, Simunovic S, Boeman RG. The effect of loading rate on the fracture toughness of fiber reinforced polymer composites. J Appl Polym Sci 2005;96:899–904.

[29] Karger-Kocsis J, Friedrich K. Temperature and strain-rate effects on the fracture toughness of poly(ether ether ketone) and its short glass–fibre reinforced composite. Polymer 1986;27:1753–60.

[30] Chu JN, Schultz JM. The influence of microstructure on the failure behaviour of PEEK. J Mater Sci 1990;25:3746–52.

[31] Trotignon JP, Verdu J, Martin CH, Morel E. Fatigue behaviour of some temperature-resistant polymers. J Mater Sci 1993;28:2207–13.

[32] Beguelin P, Kausch HH. The effect of the loading rate on the fracture toughness of poly(methyl methacrylate), polyacetal, polyetheretherketone and modified PVC. J Mater Sci 1994;29:91–8.

[33] Gensler R, Béguelin P, Plummer C, Kausch H, Münstedt H. Tensile behaviour and fracture toughness of poly(ether ether ketone)/poly(ether imide) blends. Polym Bull 1996;37:111–8.

[34] Zhang Z, Breidt C, Chang L, Friedrich K. Wear of PEEK composites related to their mechanical performances. Tribol Int 2004;37:271–7.

[35] Jones DP, Leach DC, Moore DR. Mechanical properties of poly(ether-ether-ketone) for engineering applications. Polymer 1985;26:1385–93.

[36] Wu GM, Schultz JM. Fracture of orientated poly(ether-ether-ketone). Polym Eng Sci 1989;29:405–14.

[37] Brillhart M, Botsis J. Fatigue fracture behaviour of PEEK: 2. Effects of thickness and temperature. Polymer 1992;33(24):5225.

[38] Saib KS, Evans WJ, Issac DH. The role of microstructure during fatigue crack growth in poly(aryl ether ether ketone) (PEEK). Polymer 1993; 43(15):3198–203.

[39] Kemmish DJ, Hay JN. The effect of physical ageing on the properties of amorphous PEEK. Polymer 1985;26:905–12.

[40] Hashemi S. Effect of temperature on fracture toughness of an amorphous poly(ether-ether ketone) film using essential work of fracture analysis. Polym Test 2003;22:589–99.

[41] Arkhireyeva A, Hashemi S. Effect of temperature on work of fracture parameters in poly(ether-ether ketone) (peek) film. Eng Fract Mech 2004;71:789–804.

[42] Karger-Kocsis J. For what kind of polymer is the toughness assessment by the essential work of fracture concept straightforward. Polym Bull 1996;37:119–26.

[43] Taylor GI. The use of flat ended projectiles for determining dynamic yield stress. Proc R Soc London A 1948;194:289–99.

[44] Briscoe BJ, Hutchings IM. Impact yielding of high density polyethylene. Polymer 1976;17:1099–102.

[45] Vartanov MA, Dmitrieva TA, Romanchenko VI. Dynamic properties of polycarbonate with impact of a cylinder on an obstacle. Combust Explo Shock Waves 1990;25(4):490–2.

[46] Rae PJ, Brown EN, Clements BE, Dattelbaum DM. Pressure induced phase change in poly(tetrafluoroethylene) at modest impact velocities. J Appl Phys 2005;98(6):1–8.

[47] Millett JCF, Bourne NK, Stevens GS. Taylor impact of polyether ether ketone. Int J Impact Eng 2006;32(7):1086–94.

[48] Devaux J, Delimoy D, Daoust D, Legras R, Mercier JP, Strazielle C, et al. On the molecular weight determination of a poly(aryl-ether-ether-ketone) (PEEK). Polymer 1985;26:1994–2000.

[49] Walley SM, Field JE, Pope PH, Safford NA. A study of the rapid deformation behaviour of a range of polymers. Philos Trans R Soc London A 1989;328:1–33.

[50] Gray III GT, Blumenthal WR. Split-Hopkinson pressure bar testing of soft materials. In: ASM-Handbook-Committee, editor. ASM handbook. Mechanical testing and evaluation, vol. 8. ASM International; 2000. p. 488–96.

[51] Panametrics. Ultrasonic technical notes. Technical report. <http://www.panametrics.com/>; 2001.
[52] Brown EN, Dattelbaum DM. The role of crystalline phase on fracture and microstructure evolution of polytetrafluoroethylene (PTFE). Polymer 2005;46(9):3056–68.
[53] Landes JD, Herrera R. A new look at JR analysis. Int J Fract 1988; 36:R9–14.
[54] Morhain C, Velasco JI. Determination of JR curve of polypropylene copolymers using the normalization method. J Mater Sci 2001;36(6):1487–99.
[55] Landes JD, Bhambri SK, Lee K. Fracture toughness testing of polymers using small compact specimens and normalization. J Test Eval 2003; 31(2):1–7.
[56] Joyce JA. Fracture toughness evaluation of polytetrafluoroethylene. Polym Eng Sci 2003;43(10):1702–14.
[57] Menard KP. Dynamic mechanical analysis: a practical introduction. 1st ed. Boca Raton, FL, USA: CRC; 1999.
[58] Maeda Y. Effect of pressure on the thermal behaviour of quenched poly-(etheretherketone) and poly(ethyleneterephthalate). Polym Commun 1991;32(9):279–84.
[59] Victrex. Victrex peek materials properties data table. Technical report. <http://www.victrex.com/>; 2000.
[60] Swallowe GM, Fernandez JO. Crystallisation effects during high rate deformation of polymers. J Phys IV 2000;10(9):311–6.
[61] Zhao H, Li RKY. Fracture behaviour of poly(ether ether ketone) films with different thicknesses. Mech Mater 2006;38:100–10.
[62] Ivanov DA, Jonas AA. Comparison of the alpha relaxation of amorphous poly(aryl-ether-ether-ketone) (PEEK) probed by dielectric and dynamic mechanical analysis. Polymer 1998;39:3577–81.